Int. J. Heat Mass Transfer. Vol. 26, No. 10, pp. 1439–1452, 1983
Printed in Great Britain

0017-9310/83 $3.00 + 0.00

TRANSPORT NEAR A VERTICAL ICE SURFACE MELTING IN WATER OF VARIOUS SALINITY LEVELS

B. SAMMAKIA and B. GEBHART
Department of Mechanical Engineering & Applied Mechanics, University of Pennsylvania, Philadelphia, PA 19104, U.S.A.

(*Received for publication* 1 *February* 1983)

Abstract—The results of an experimental investigation of the buoyancy driven flow adjacent to a vertical ice surface melting in saline water are presented. Several ambient water salinities, s_∞, are studied, namely 14‰, 17‰, 22‰, 30‰ and 35‰. For each salinity level, several ambient water temperatures, t_∞, are investigated, ranging from $t_\infty = -1.75$°C when $s_\infty = 35$‰ to $t_\infty = 17$°C when $s_\infty = 17$‰. Time exposure photographs of the flow field show that several distinctively different regimes of flow occur, depending on both the ambient water salinity level and temperature. At all of the salinities considered in the present study, the flow is observed to be laminar at low ambient water temperatures. This laminar flow is either upward, at the low salinity levels, or bi-directional at the higher salinities. At intermediate ambient water temperatures the flow is observed to be bi-directional and laminar over the lower portion of the ice surface, and upward and turbulent over the top portion of the ice surface. As the ambient water temperature is further increased the flow is seen to split, with a downward moving turbulent layer over the lower portion of the ice surface, and an upward moving layer over the top portion. The complicated nature of this type of flow is due to the interaction of two buoyancy force components, namely that due to salinity gradients and that due to thermal gradients. These forces are aiding or opposing, depending on the ambient water salinity level and temperature. Also, each of these forces exerts itself across a different thickness of the total boundary region. Velocity profiles, measured from the time exposure photographs, are presented and shown to be in good agreement with the analytical results of Carey and Gebhart [1, *J. Fluid Mech.* **107**, 37–55 (1981)]. Measured solid–liquid interface temperatures and inferred interface salinities are also presented for the different salinity levels and ambient water temperatures.

NOMENCLATURE

f'	non-dimensional velocity function
g	acceleration due to gravity
Gr	Grashof number defined by equation (4)
$\bar{h}$	average coefficient of heat transfer
h_{il}	specific heat of fusion of ice
k	thermal conductivity
L	length of ice surface
$\dot{m}$	melting rate of ice surface $(t_m - t_\infty)/(t_0 - t_\infty)$
Nu	average Nusselt number
P	pressure [bars absolute]
R	$(t_m - t_\infty)/(t_0 - t_\infty)$
S	salinity level
t	temperature
u	velocity component in x-direction
W	width of the ice surface
$\bar{x}$	vertical distance along the surface
$\bar{y}$	horizontal distance normal to the surface

Greek symbols

β	volumetric coefficient of thermal expansion
ν	kinematic viscosity

Subscripts

il	ice–liquid interface
0	at the surface
m	at extremum temperature
∞	in the undisturbed fluid

1. INTRODUCTION

THE COMPLICATED transport phenomena arising in the buoyancy induced flow adjacent to an ice slab melting in fresh water have been extensively investigated in the past. Such flows have been considered both experimentally and analytically for spherical, cylindrical and flat surfaces [2, 3].

However, most of the few previous investigations of ice melting in saline water were conducted at or near oceanic salinities. Johnson [4] determined some of the melting characteristics of a flat vertical ice slab immersed in water at a salinity level, s_∞, of 35‰, for ambient temperatures from −1.08 to 24.4°C. Both a differential thermocouple and a Schlieren system were used to infer flow direction. It was surmised to be always upwards. The flow was said to be laminar at low ambient temperatures. Transition to turbulence arose at higher ambient water temperatures.

In an extensive study of the same type of flow, Josberger and Martin [5] illuminated suspended particles in water at near oceanic salinity to visualize the flow, for ambient water temperatures ranging from −1.15°C to 26°C. Several distinctive overall flow regimes were seen, depending on ambient water temperature. Josberger and Martin also conducted some experiments at lower salinities, at $s_\infty = 14.2$‰ and 8‰, for low ambient water temperatures, and report observing fully laminar upward flow at both salinity levels.

Carey and Gebhart [1] report the results of numerical calculations for the laminar buoyancy flows driven by the thermal and saline transport arising near a vertical ice surface melting in saline water. Solutions were found to be possible only to $s_\infty = 31$‰, at low temperatures and only at very low salinities at high temperatures, to 20°C. Subsequently Carey and Gebhart [6] report the results of a visualization

experiment, at $s_\infty = 10‰$, in which time exposure photographs are used to visualize the fine details of the flow generated adjacent to a vertical melting ice surface. Six ambient water temperatures, t_∞, were studied, across the range from 1 to 15°C. Several very different flow characteristics were seen. From these experimental results, in the light of previous experimental data, they surmise that six different flow regimes occur. The whole flow region, in terms of s_∞ and t_∞, is divided into possible sub-regions, each characterized by a certain type of flow, as shown in Fig. 1. In Region Ia a simple melt-driven upward boundary-layer flow occurs. Region IIa is characterized by a bi-directional laminar flow, with an upward moving layer near the surface and a downflow on the outside. In Region IIb the flow is observed to split on the outside, resulting in a bi-directional flow over the lower portion of the surface and an upward flow over the top portion. In this region the upward moving layer near the surface undergoes transition to turbulence near the top of the ice surface. The flow also splits in Region IIc, however, in this region the flow splits near the top of the surface, and a turbulent downflow is observed over most of the ice surface.

Also shown in Fig. 1 are lines of constant $R = \{[t_m(s_\infty) - t_\infty]/t_0(s_0) - t_\infty]\}$. The value of R indicates the nature of the local variation and direction of the thermal buoyancy force, since it places the specific temperature conditions, t_0 and t_∞, with respect to $t_m(s, p)$. The role of R as the quantitative expression of the effect of the extremum behavior is discussed in detail by Carey and Gebhart [1]. Lines of constant R are seen to originate at the intersection of the ice melting temperature line $t_{il}(s_\infty)$ and the extremum temperature line $t_m(s_\infty)$. All negative values of R occur within the narrow triangle bounded by t_{il} and t_m, namely Region Ia in Fig. 1.

In this study, a detailed investigation of flow and transport is made for ambient water salinities ranging from $s_\infty = 14‰$ to $35‰$. Various ambient water temperatures were used at each salinity level, ranging from $t_\infty = -1.75$°C to 17°C. This range of salinities had not been investigated experimentally in detail previously, although many environmental and technological applications arise in these ranges of s_∞ and t_∞. Salinities lower than oceanic often arise in nature in the vicinity of large masses of ice melting in the ocean and in esturine waters.

The second author recently had an opportunity to gather water samples in bays and channels near tidal ice at Juneau and in Glacier Bay in Alaska, as a guide to subsequent realistic studies of ice melting in saline water. The salinities of eight samples are shown in Table 1. Some levels are very much lower than oceanic salinity. They are also quite variable with both location and tidal motion. These results are a reminder that salinity is very commonly a primary variable. The NORSEX research expedition into the marginal ice zone of the Arctic ice pack, in late 1979, also concerned ice melting characteristics. Salinity and temperature measurements indicated that water temperatures as low as −1.75°C, and reduced salinities are very common [7].

In this study, the ice–liquid interface temperatures, t_0, were measured for the different ambient water salinities and temperatures. From t_0 measurements the water–ice interface salinity, s_0, was inferred using the phase equilibrium equation of Fujino *et al.* [8]. Melting rates and velocity profiles are computed from the time exposure photographs of the flow field. These results are compared to the analytical results of Carey and Gebhart [1], where the latter are applicable.

2. EXPERIMENT

In this study of the flow regimes resulting from ice melting in saline water, the relevant parameters are ambient water salinity and temperature. The experi-

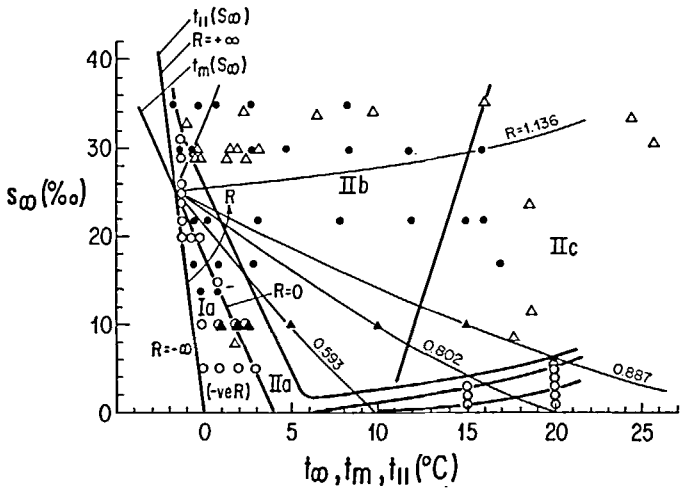

FIG. 1. Flow regimes corresponding to ambient water salinity and temperature. Also shown are several lines of constant R. The experimental points are Josberger and Martin [5] △, Carey and Gebhart [6] ▲, the present study ●. The conditions for the calculations of Carey and Gebhart [1] are shown by ○.

Table 1. Measured salinities near Juneau (J) and in Glacier Bay (GB) in Alaska, 27–30 May 1979

Location	Date/Tide	Salinity (‰)
1. J., Gastineau Channel	30 May, 11:40 am, low tide	21.45
2. J., Gastineau Channel	30 May, 6:50 pm, high tide	17.40
3. GB, Bartlett Cove	27 May, 9:35 pm, low tide	31.27
4. GB, Bartlett Cove	28 May, 5:10 pm, high tide	32.09
5. GB, near Marble Island South	27 May, 5:00 pm	32.76
6. GB, near Marble Island North	27 May, 6:00 pm	32.16
7. GB, at Riggs Glacier Outside bar	27 May, 8:00 pm	20.88
8. In ice bits near surface	27 May, 8:00 pm	18.94

ments were conducted in a glass tank 86 cm deep, 69 cm long and 66 cm wide. The desired ambient water salinity was achieved by using de-ionized water to dilute an artificial 35‰ sea water solution. The precise recipe used to make this solution (Table 2) is from Lyman and Fleming [9]. Johnson [4] checked the electrical conductivity of a 35‰ solution made according to this recipe against that of a standard sample of sea water, from the Institute of Oceanographic Sciences in Wormley, Godalming, Surrey, U.K., the electrical conductivities indicated that salinities were in agreement to within 0.2‰.

Before each subsequent experimental run the salinity of the ambient water was checked by measuring the electrical conductivity of the tank water, and that of water at 35‰ salinity. A Beckman RC19 Conductivity Bridge and Dip Cell were used for all conductivity measurements. Knowing the ratio of the two conductivities, the exact salinity of the tank water could then be calculated using the Joint Panel on Oceanographic Tables and Standards (JPOTS) tables. The salinity was then increased or decreased to the required level by adding a concentrated solution prepared according to the above mentioned recipe, or de-ionized pure water, as required.

The tank temperature was then reduced to the desired ambient temperature. An immersion chiller was used, while stirring the tank water. The tank was insulated by a 2.4 cm thick layer of polyurethane insulation, covered by a 7.6 cm layer of fiberglass insulation. After the required ambient temperature was reached, the chiller was removed, and the tank was stirred for 10–15 min to ensure a uniform temperature distribution. After stirring, approximately 40 min were allowed before inserting the ice and starting the experiment, to ensure the quiescence of the ambient water.

Table 2. Recipe for 35‰ artificial sea water

Ingredients	Amount (g)
NaCl	29.939
$MgCl_2$	5.079
Na_2SO_4	3.994
$CaCl_2$	1.123
KCl	0.667
$NaHCO_3$	0.027
KBr	0.098
H_3BO_3	0.027

And fill with distilled water to become 1 kg of solution.

The ice slabs were made by placing an acrylic plastic rectangular frame in a shallow aluminum pan with a smooth 6 mm thick bottom. The frame was 2.5 cm deep, 20.35 cm wide, and 27.5 cm long and lined on the inside with expanded polystyrene insulation. Vigorously boiled de-ionized water would then be gently poured into the pan, to avoid excessive exposure to air. The top and sides of the pan would then be insulated, and the pan would then be placed in a freezer. The water froze from the bottom upwards. By following this procedure, the ice surface formed at the bottom of the pan would be smooth and free of gas bubbles. Any remaining gas in the water would rise towards the top surface during the freezing process. The ice surfaces were 18.4 cm wide, 23.2 cm high and 3 cm thick. During the experiments the ice was held in place by means of two stainless steel rods which passed through four stainless steel 'guides' attached to the corners of the plastic frame. The two rods were attached at the top to a flat Plexiglass base which rested on three levelling screws, thus the ice could be made to stand vertically in the tank, at an accuracy of approximately 2°.

Three 0.013 cm diameter copper–constantan thermocouples were embedded in the ice (Fig. 2), where two of them were positioned just inside the original ice surface. A Hewlett Packard 3455A model digital voltmeter was used to read the temperature, also recorded by a Hewlett Packard 5150A model thermal printer. Before inserting an ice slab into the tank, the temperature was brought up to the expected interface temperature t_0 that would accompany melting, at the values of s_∞ and t_∞. This was accomplished by lightly insulating the ice slab and leaving it in room temperature surroundings. Meanwhile the temperature of the slab was monitored by means of the three imbedded thermocouples until it reached an estimated t_0, uniformly. During the experiment the actual resulting interface temperature was measured by

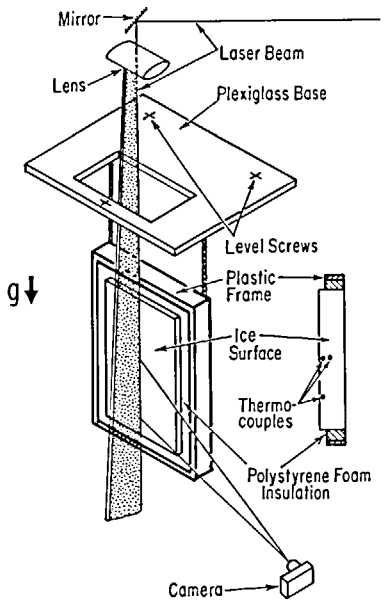

FIG. 2. Schematic diagram showing the relative positions of the ice surface, laser beams, and the camera.

visually observing the thermocouple beads as they broke through the receding ice surface.

The flow was visualized by adding 2 g of pliolite, ground to 40 μm size, to the water. A collimated horizontal beam produced by a horizontal 5 mW helium neon laser was first reflected off of a first surface mirror positioned at a 45° angle. The vertical beam was then spread into a plane of about 2 mm thickness by a cylindrical lens. This plane beam, about 60 mm wide, was aligned perpendicular to the ice surface (Fig. 2). Side scatter of this beam, off of the pliolite particles, made them visible, thereby visualizing the flow. A motor driven 35 mm Nikon camera was used to take time exposure photographs. An intervalometer was used to control the time exposure and the interval between different photographs.

3. RESULTS AND DISCUSSION

When ice melts in saline quiescent water, the resulting buoyancy induced flows are of a very complicated nature. The two diffusive buoyancy forces which arise, of temperature and of salinity, interact to produce several distinctively different regimes of flow. The buoyancy force due to salinity diffusion is always acting upwards when pure water ice melts in saline water. However, the thermal component of the buoyancy force may be of a more complex nature, arising from an anomalous density variation of water as a function of temperature. At atmospheric pressure, and for a local water salinity of about $25°/_{oo}$ or more, at 1 bar pressure, the temperature at which density extremum would occur, $t_m(s)$, is lower than the melting temperatures at that salinity $t_{il}(s)$. Thus, for salinities greater than about $25°/_{oo}$ throughout the region, the thermal buoyancy force will always be downward and opposed to the saline buoyancy force. Since the Lewis number, $Le = Sc/Pr$, is large for saline diffusion in water, the resulting buoyancy force distribution is expected to always be bi-directional.

Figures 3(a)–(d) show the flow regimes which arose for an ambient water salinity of $35°/_{oo}$ at ambient water temperatures of -1.75, 1, 3 and 8.5°C, respectively. Figure 3(a) is a 120 s time exposure, at $t_\infty = -1.75$°C. The flow can be seen to be bi-directional over the entire length of the ice slab. Near the ice surface it is a thin upward moving layer. In this thin region, close to the ice surface, the buoyancy force due to salinity gradients dominates and causes this upward motion. This same flow regime was observed by Josberger and Martin at $(s_\infty, t_\infty) = -1.15$°C, $33°/_{oo}$.

Under these circumstances the Schmidt number is about 3170. The Prandtl number is only about 13.9, therefore, $Le \approx 228$. Thus, the thermal buoyancy force, although weaker than the saline buoyancy force, has a much wider domain of influence. This causes the significantly thicker downward moving layer on the outside. Under close inspection it can be seen that the upward moving layer next to the surface entrains fluid from the downward flowing layer over the entire vertical length of the slab. That is, fluid moving downward changes direction by almost 180° as it is entrained in the upward moving layer. Turning points can be observed over the entire vertical length of the slab. Thus this is Region IIa as predicted by Carey and Gebhart [6] should be extended to include higher salinities at low temperatures as shown in Fig. 1. As the ice slab melts from both sides, the two upward moving layers apparently join at the top and their wakes form a single rising buoyant plume. The downward moving layer clearly originates near the top of the slab, and continues to entrain more fluid as it moves downwards, thus increasing in thickness. Near the center-height of the ice slab the ratio of the thickness of the upward moving layer to the downward one was measured to be approximately 1/10. Both layers are seen to be laminar over the entire flow field.

Figure 3(b) is a 60 s time exposure at $t_\infty = 1$°C. The flow behavior is remarkably different from that occurring at -1.75°C. There remains an inner upward moving layer over the whole slab. However, it is turbulent over about the upper half of the ice slab. On the other hand, the outer downward layer can be seen to split approximately 3/4 up the slab, to upward flow. Thus, the flow adjacent to the lower portion of the ice slab is bi-directional and basically laminar. This observation is confirmed by the smoothness of the lower portion of the ice slab after considerable melting had occurred. The upper portion of the slab, however, eventually developed vertical longitudinal depressions, indicating the presence of streamwise vortices. Near the slab the saline buoyancy force still dominates the flow and causes the upward motion. At approximately mid-height this upward moving layer becomes unstable and undergoes transition to turbulence. The downward thermal buoyancy force is overcome by saline driven

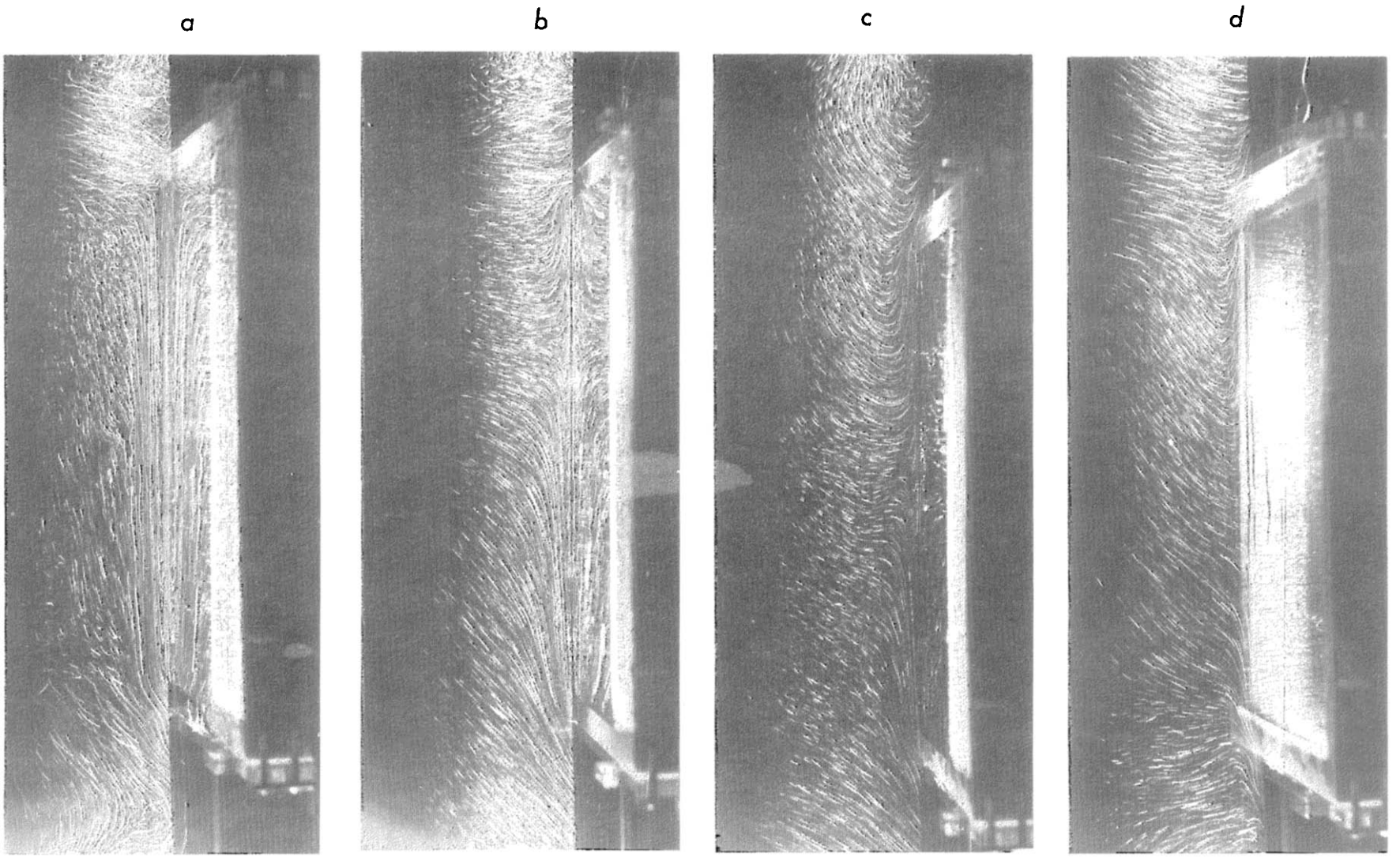

FIG. 3. Flow adjacent to a vertical ice slab melting in saline water at $s_\infty = 35°/_{oo}$. Ambient water temperatures and exposure times are: (a) −1.75°C, 120 s. (b) 1°C, 60 s. (c) 3°C, 40 s. (d) 8.5°C, 40 s.

upward turbulent flow. However, when acting over a thicker and laminar layer, it still causes downward motion over the lower part. A concentrated horizontal entrainment, similar to that first seen by Josberger and Martin [5] supplies this divided outer flow. An almost identical flow behavior to this was observed by Carey and Gebhart [6] at ambient conditions of $10°/_{oo}$ but at $t_\infty = 5°C$, also Region IIb.

For $t_\infty = 3°C$, the flow regime [Fig. 3(c)] differs little from that seen at 1°C. The outer flow still splits, but at a lower point. The outer downflow now occupies approximately the lower half of the ice surface and is apparently still laminar. Also, over the top portion of the ice slab the outer flow turns from downward to upward and becomes turbulent.

Figure 3(d) is a 40 s time exposure of the flow for $t_\infty = 8.5°C$. The splitting point for the outer flow can be observed to be even lower than that for $t_\infty = 3°C$. Also the flow adjacent to the lower portion of the surface is completely downward and laminar, while the flow over the top portion of the surface is again bi-directional, turning into a turbulent flow near the ice surface. The vertical ridges mentioned earlier can be observed upon close inspection of Fig. 3(d). These ridges are seen to be most prominent near the splitting point of the outer flow. At that location the warmer ambient fluid is entrained and comes directly inward towards, and perhaps to, the ice surface. The melting rate was considerably higher for this circumstance than for the previous three.

In summary, for $s_\infty = 35°/_{oo}$ the flow is laminar and bi-directional when $t_\infty = -1.75°C$. As t_∞ increases the outer downward flow splits, and the inner upward moving layer undergoes transition from laminar to turbulent flow. As t_∞ is further increased the splitting point in the outer flow shifts to a lower location and the upward moving inner layer can be observed to exist only over the upper section of the ice slab.

It is seen in Fig. 4 that some differences arise as salinity is reduced to $30°/_{oo}$. Note that a temperature-caused density extremum and a buoyancy force inversion both become more likely at reduced s, in the melt.

Figure 4(a), for $t_\infty = -1°C$, is similar to that for $s_\infty = 35°/_{oo}$ and $t_\infty = -1.75°C$, as shown in Fig. 3(a). However, the outer downflow layer is noticeably thicker at $s_\infty = 30°/_{oo}$. This is due to a deeper penetration of the thermal buoyancy force into the ambient fluid. This trend of increasing thickness continues to lower salinities as well. Note however that the flow is still bi-directional and apparently laminar over the entire height of the ice surface. In Fig. 4(b) the ambient water temperature was $-0.25°C$. In Fig. 1 this curcumstance was predicted by Carey and Gebhart [6] to lie in Region IIb. The outer downward flow splits very near the top of the ice slab and the inner upward flow is seen to be turbulent near the top of the slab. Thus it appears that the line separating Regions IIa and IIb is quite accurately predicted, at this salinity level.

Figures 4(c) and (d) show the resulting flow regimes for $t_\infty = 8.7°C$ and 16°C, respectively. Under both circumstances the flow splits on the outside. At 8.7°C the still laminar downward lower flow is seen to cover a smaller section of the ice surface than at $t_\infty = -0.25°C$. Also long vertical ridges are seen over the top portion of the ice surface. The top portion also melted at a faster average rate than the lower portion.

At 16°C the flow is quite different. Most of the surface is covered by a turbulent downflow and only a very small section near the top of the surface is bi-directional. Clearly the thermal buoyancy force has almost completely overcome the saline buoyancy force and the result is a turbulent downflow over most of the ice surface. Note also that the surface of the ice has become very irregular during melt. This indicates strong variations in the local rate, due to the turbulent nature of the flow. This regime, Region IIc in Fig. 1, was observed by Josberger and Martin [5] and by Carey and Gebhart [6]. Thus at an ambient water salinity of $30°/_{oo}$ the resulting flow regimes are observed to be similar to those occurring at $35°/_{oo}$. In bi-directional flow the downward moving layer is thicker. In the split flow regime the splitting point is also found to shift downwards with increasing ambient temperature.

In Figs. 5(a)–(d), the flow regimes are shown for an ambient water salinity of $22°/_{oo}$. The flow regime at $t_\infty = -0.5°C$ [Fig. 5(a)] has the same basic characteristics as those at $s_\infty = 35°/_{oo}$ and $t_\infty = -1.75°C$ and at $s_\infty = 30°/_{oo}$ and $t_\infty = -1°C$. However, here the downward moving outer layer is much thicker. The downward acting thermal buoyancy force clearly exerts itself deeper into the ambient fluid. The completely bi-directional flow is clearly seen in Fig. 5(a). The inside upward moving layer is moving at a higher velocity than that of the outer downward flow. The whole field is laminar. The outer layer entrains fluid mostly near the top of the ice slab. While some of this fluid is entrained to form the inner layer, which changes direction and moves upwards. However, most of it is shed at the bottom of the slab forming a descending plume. Very close inspection of the upward moving layer very close to the surface, reveals zig-zag particle tracks. This is a 2-dim. projection into the plane of illumination of a particle moving upwards in a helical path. Figure 6 is an enlargement of a 20 s exposure of this flow circumstance. The helical motion is seen to occur at several locations along the ice slab, even near the leading edge. It appears that the flow picks up disturbances from the surroundings which eventually dampen out due to the stability of the flow. A further indication of a laminar flow is that the ice surface remains smooth during the melting process indicating a transversely uniform local melting rate.

Figure 5(b) is a 40 s exposure of the flow regime at $t_\infty = 2.5°C$. The flow splits with a bi-directional flow over the lower section of the slab and an inner upward moving layer that undergoes transition to turbulence adjacent to the upper portion of the slab. This type of flow is similar to that occurring at $s_\infty = 35°/_{oo}$ and $t_\infty = 1°C$ and also at $s_\infty = 30°/_{oo}$ and $t_\infty = -0.25°C$.

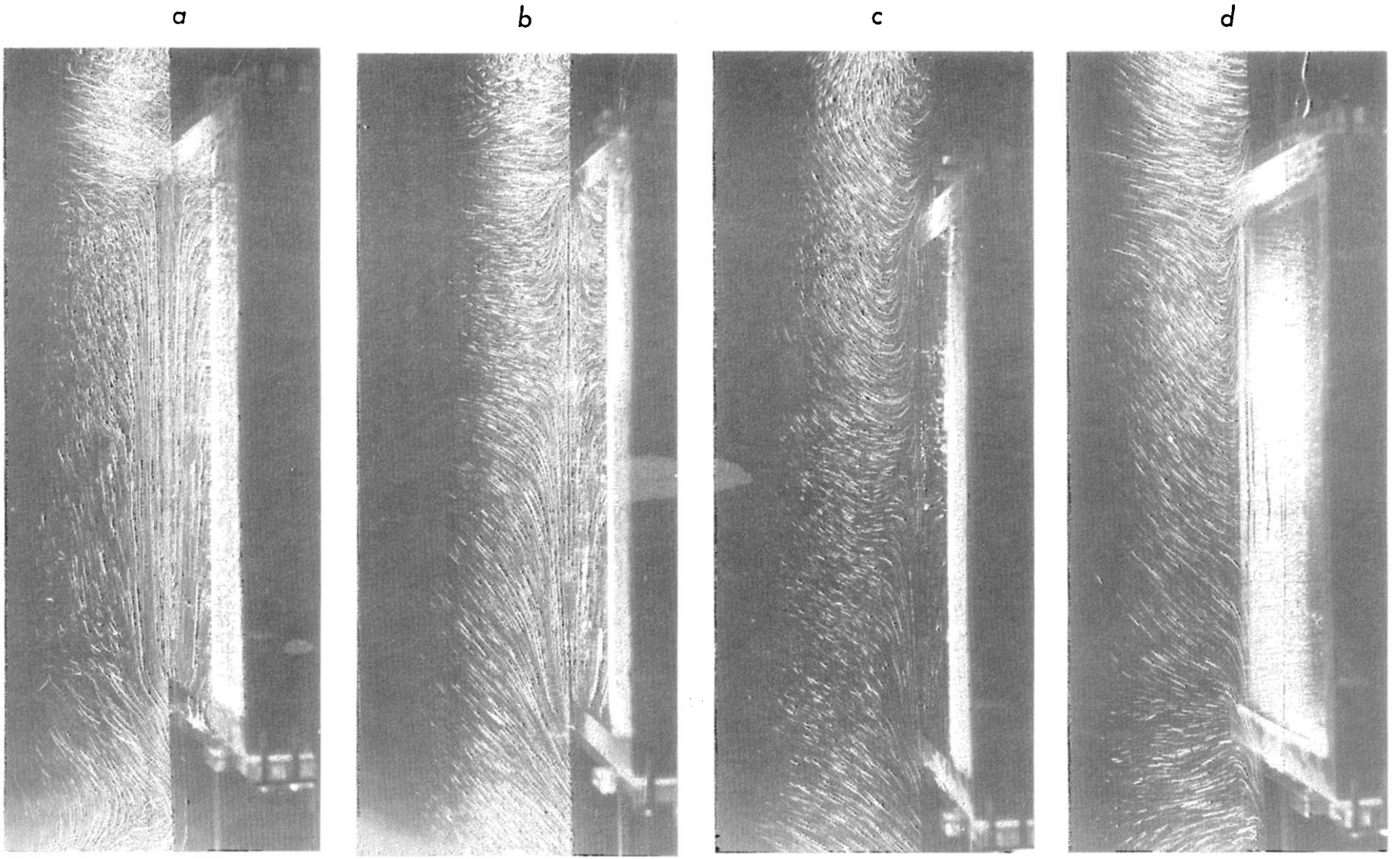

FIG. 4. Flow adjacent to a vertical ice slab melting in saline water at $s_\infty = 30‰$. Ambient water temperatures and exposure times are: (a) −1°C, 60 s. (b) −0.25°C, 30 s. (c) 8.7°C, 40 s. (d) 16°C, 30 s.

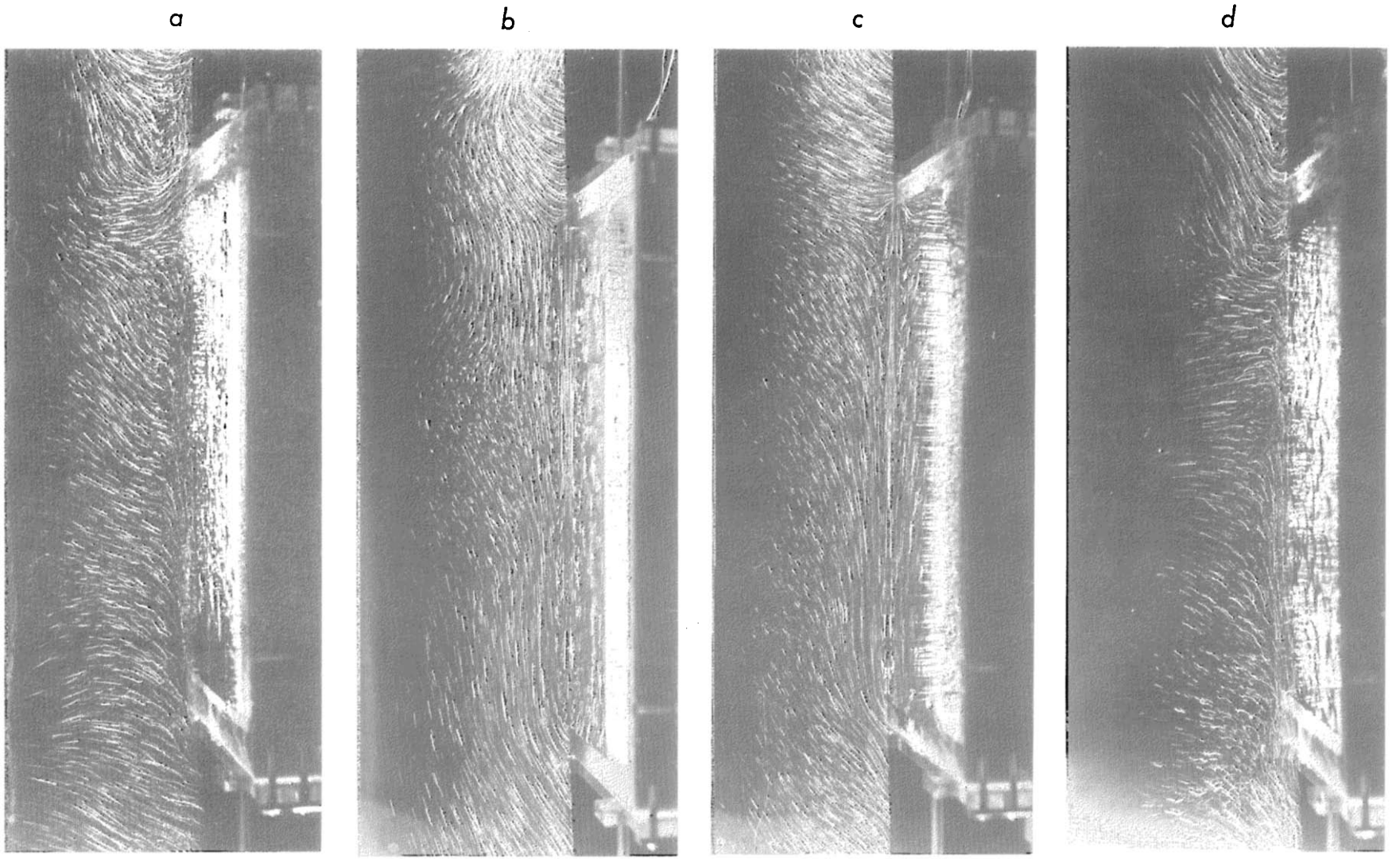

FIG. 5. Flow adjacent to a vertical ice slab melting in saline water at $s_\infty = 22‰$. Ambient water temperatures and exposure times are: (a) -0.5°C, 60 s. (b) 3.2°C, 40 s. (d) 8°C, 20 s. (d) 16°C, 30 s.

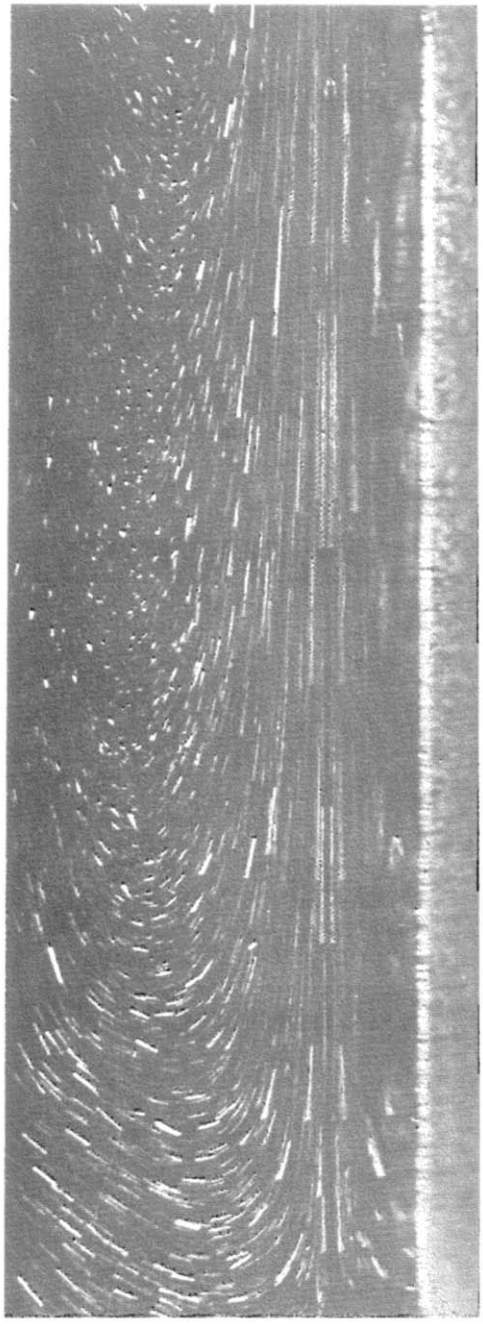

FIG. 6. Flow adjacent to a vertical ice slab melting in saline water where $s_\infty = 22°/_{oo}$, $t_\infty = -0.5°C$ and the exposure time = 20 s.

Figures 5(c) and (d) are for $t_\infty = 8°C$ and 16°C, respectively. At 8°C the flow is similar to that at $s_\infty = 35°/_{oo}$ and $t_\infty = 8.7°C$ and at $s_\infty = 30°/_{oo}$ and $t_\infty = 8.7°C$. Here also the melt rate is higher near the splitting point of the outer flow. Also, the same type of long vertical longitudinal ridges are seen in the ice surface. At $t_\infty = 16°C$ the flow is similar to that occurring at $s = 30°/_{oo}$ and $t_\infty = 16°C$. Again the ice surface melted in a very irregular fashion, indicating large scale turbulence over most of the ice surface.

Figures 7(a)-(c) are the flows which result at $s_\infty = 17°/_{oo}$ at $t_\infty = 1°C$, 3°C and 17°C, respectively. At 1°C the flow is bi-directional and laminar, with an inner layer moving at a velocity relatively higher than that of the downward moving outer layer. This type of flow is similar to that at $s = 35°/_{oo}$ and $t_\infty = -1.75°C$, $s_\infty = 30°/_{oo}$ and $t_\infty = -1°C$ and at $s_\infty = 22°/_{oo}$ and $t_\infty = -0.5°C$. At $t_\infty = 3°C$ the flow splits on the upper portion of the ice slab. Again the lower portion of the slab is exposed to a bi-directional flow, and the inner upward moving layer undergoes transition to turbulent flow near the top of the slab. This is similar to that at $s_\infty = 35°/_{oo}$ and $t_\infty = 1°C$, at $s_\infty = 30°/_{oo}$ and $t_\infty = -0.25°C$ and at $s_\infty = 22°/_{oo}$ and $t_\infty = 3.2°C$. The same regime is also reported by Carey and Gebhart [6] at $s_\infty = 10°/_{oo}$ and $t_\infty = 5°C$.

Figure 7(c), at $t_\infty = 17°C$, is downward and turbulent over most of the surface. This indicates that the thermal buoyancy force at 17°C is dominating the flow. Again note the ice surface is seen to be very irregular, due to turbulence, as observed at $s_\infty = 30°/_{oo}$ and $t_\infty = 16°C$ and at $s_\infty = 22°/_{oo}$ and $t_\infty = 16°C$. Figure 7(d) is a 15 s time exposure of the flow when $s_\infty = 14°/_{oo}$ and $t_\infty = 0°C$. The flow is seen to be laminar and fully upward. This results because both the temperature and salinity components of the buoyancy force act upwards. More observations were made at this salinity and at higher ambient water temperatures. At $t_\infty = 4°C$ the flow regime was very similar to that at $s_\infty = 17°/_{oo}$ when $t_\infty = 3°C$, while $s_\infty = 14°/_{oo}$ and $t_\infty = 13.0°C$ produce a flow configuration similar to that occurring at $s_\infty = 17°/_{oo}$ and $t_\infty = 16°C$.

Figure 8 is a plot of the measured interface temperature, t_0, for the experiment at different ambient temperatures and salinities. Also plotted are the inferred interface salinities, s_0, calculated from t_0 by using the following relation developed by Fujino *et al.* [8], as corrected:

$$t_0 = t_{il}(s,\ p) = -0.02831 - 0.0499 s_0 - 0.000112 s_0^2 - 0.00759 p. \quad (1)$$

In equation (1), s_0 is the ambient water salinity and p is the pressure in bars absolute. The values of s_0 are collected in Table 3. The temperature t_0 was measured at two different locations along the ice surface, at 6 cm and 11.6 cm from the bottom of the slab. At low ambient water temperatures these two temperature readings were essentially the same. In the intermediate ambient water temperature range, when the flow split and was laminar over the lower portion of the ice slab, the difference in the two readings remained less than 0.05°C. In Fig. 8 it is seen that the interface temperature increased monotonically with increasing ambient water temperature at any given salinity level. Thus s_0 decreases with increasing t_∞, reflecting the increased melting rates at higher t_∞.

Successive photographs also provide quantitative information about flow field velocities and local heat transfer rates. During the experiments the camera was

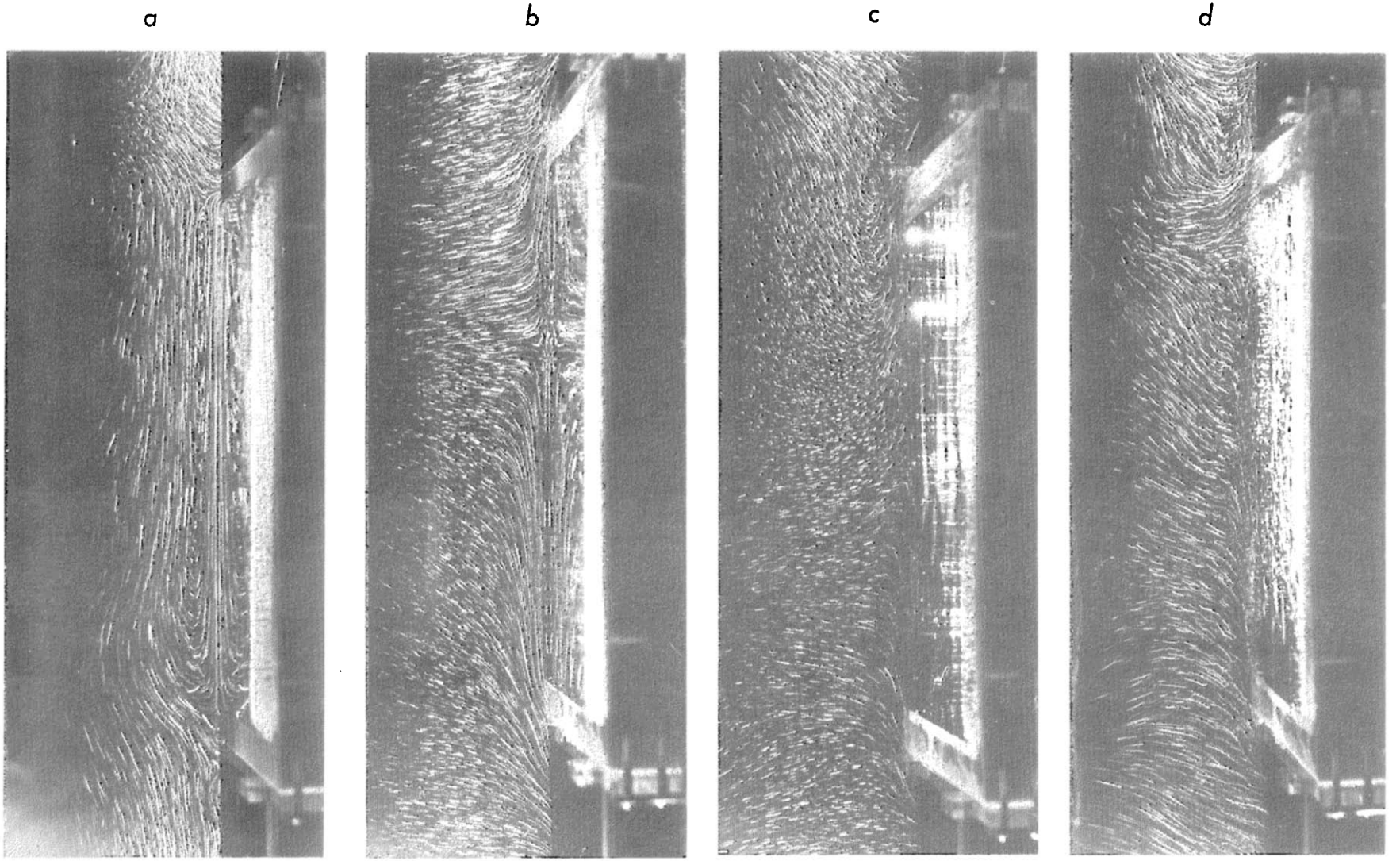

FIG. 7. Flow adjacent to a vertical ice slab melting in saline water. Ambient water salinities, temperatures, and time exposures are: (a) 17‰, 1°C, 15 s. (b) 17‰, 3°C, 30 s. (c) 17‰, 17°C, 30 s. (d) 14‰, 1°C, 20 s.

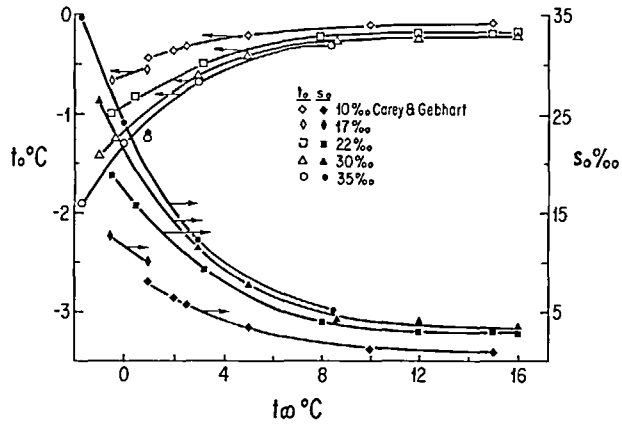

FIG. 8. Measured interface temperatures and inferred salinities for the different ambient water salinities and temperatures.

placed at a small angle to the ice surface (Fig. 2). Thus, the reflection of the illuminated particles off of the ice surface is also visible in the photographs. By bisecting the distance between pairs of images the exact location of the ice surface is found. Thereby, melting rates are determined. The projected length of a particle streak, measured using a precision scale, divided by the exposure time, yields the velocity u. The distance perpendicular to the surface, $\bar{y}$, is also measured. To determine the streamwise location, $\bar{x}$, the distance from the center of the stream to the leading edge is measured. Due to the angle between the line of camera sighting and the ice surface, some correction is necessary, both for the aximuthal and altitude angle effects. The distance between the plane of light and the camera also enters into these angle corrections. The corrected

Table 3. The measured surface temperature (t_0) for the different experimental conditions. Also shown are the inferred interface salinities and the non-dimensional temperature parameter $R = (t_m - t_\infty)/(t_0 - t_\infty)$

s_∞ (‰)	t_m (°C)	t_∞ (°C)	t_0 (°C)	s_0 (‰)	$R = \frac{t_m - t_\infty}{t_0 - t_\infty}$	Nu
		1	−0.44		−0.631	
		2	−0.36		0.0389	
10	1.908 [1]	2.5	−0.33		0.2092	
		5	−0.21		0.5935	
		10	−0.09		0.802	
		15	−0.08		0.8775	
14	1.0596	0°C	−0.58	10.55	−1.8269	
17	0.4233	−0.5	−0.68	12.65	−4.9908	
		1.0	−0.55	10.07	0.3271	
		−0.5	−1.0	18.55	0.2744	
		0.5	−0.85	15.75	0.8423	
		3.2	−0.5	9.11	1.0371	
22	−0.6327	8	−0.22	3.75	1.0501	
		12	−0.19	3.07	1.0367	
		15	−0.19	3.07	1.0294	
		16	−0.17	2.77	1.0285	
		−1.0	−1.42	26.13	3.1762	
		−0.25	−1.25	23.133	2.084	51.8
		3.0	−0.63	11.605	1.4694	94.9
30	−2.334	5.0	−0.42	7.662	1.3518	117.1
		8.7	−0.25	4.250	1.2328	
		12.0	−0.24	4.06	1.1711	
		16.0	−0.21	3.46	1.1310	
		−1.75	−1.9	34.65	10.9633	15.0
		0	−1.3	24.03	2.6111	69.9
35	−3.3945	1	−1.25	23.13	1.9531	74.1
		3	−0.67	12.48	1.7423	97.8
		8.5	−0.3	5.22	1.3516	

velocities and distances were converted to the similarity variables appearing in the analysis of Carey and Gebhart [1] as follows:

$$f' = \frac{u\bar{x}}{2\nu\, Gr_{\bar{x}}^{1/2}}, \tag{2}$$

$$\eta = \frac{\bar{y}}{\bar{x}}(Gr_{\bar{x}}/4)^{1/4}, \tag{3}$$

$$Gr_{\bar{x}} = \frac{\rho_m(0,1)}{\rho_m(s_\infty,1)}\frac{g g_{10}\bar{x}^3(s_\infty - s_0)}{\nu^2} \tag{4}$$

where $\bar{x}$ and $\bar{y}$ are the instantaneous downstream and surface-normal coordinates, and u is the velocity component parallel to the surface. The constants g and ν are the gravitational acceleration and kinematic viscosity, respectively. The values of $\rho_m(0,1)/\rho_m(s_\infty,1)$ and g_{10} are determined from the density correlation of Gebhart and Mollendorf [2] as

$$\rho_m(0,1)/\rho_m(s_\infty,1) = \frac{1}{(1+g_{10}s_\infty)} \tag{5}$$

where

$$g_{10} = 8.046157\ E\text{-}04. \tag{6}$$

Figure 9 shows the resulting data points for the two different circumstances, at $(s_\infty, t_\infty) = (30‰, -1°C)$ and $(22‰, -0.5°C)$. Also shown is a computed curve for the $(30‰, -1.0°C$ circumstance) from the analysis of Carey and Gebhart [6]. Good agreement is seen between the 30‰ data and calculations, near the surface where the flow is upward. However, close examination of Figs. 3(a), 4(a), 5(a) and 6(a) reveal that the source of the downward outer flow is, in part, the warmer fluid being shed by the plume above the ice surface. This reduces the buoyancy force and also the outer velocity levels, as seen in Fig. 9. This is a consequence of the finite height of the ice surface. The analysis assumes an infinite surface, which precludes this outer downflow.

Heat transfer rates are estimated by measuring the recession Δl, of the ice–water interface during a given time interval $\Delta\tau$. From two photographs taken at

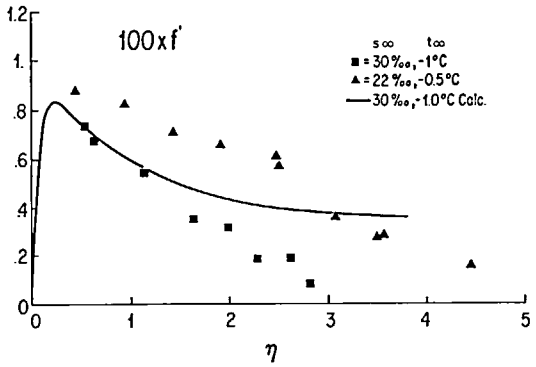

FIG. 9. Measured velocity profiles for $(s_\infty, t_\infty) = (30‰, -1°C)$ ■ and $(s_\infty, t_\infty) = (22‰, -0.5°C)$▲. Also shown are the computed results of Carey and Gebhart [1] ——.

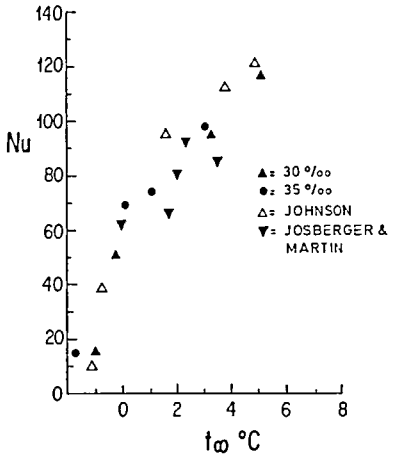

FIG. 10. Measured average heat transfer as a function of s_∞ and t_∞. $s_\infty = 35‰$ ●, $s_\infty = 30‰$ ▲, also shown are Johnson's measurements at $35‰$ [4] △, and those of Josberger and Martin [5] ▼.

different times, local and average melt rates may be determined. The average convection coefficient $\bar{h}$ is then

$$\frac{\bar{h}L}{k} = Nu = \left(\frac{\overline{\Delta l}}{\Delta\tau}\right)\frac{\rho_i h_{il}}{(t_\infty - t_0)}\frac{L}{k} \tag{7}$$

where ρ_i is the ice density, k is the thermal conductivity of water, h_{il} is the specific heat of fusion of ice and $(\overline{\Delta l}/\Delta\tau)$ is calculated from averages of the local values of Δl for several x locations, over a single interval $\Delta\tau$.

Table 3 lists the resulting values for Nu. However, Nu for $s_\infty = 35‰$, $t_\infty = -1.75°C$, was determined by weighing the ice slab before and after immersion. In this method the Nusselt number is calculated from the weight loss rate per unit area,

$$Nu = \frac{\dot{m}h_{il}}{2kW(t_\infty - t_0)}. \tag{8}$$

The measured average Nusselt numbers at $35‰$ and $30‰$ are plotted in Fig. 10 for various ambient temperatures. Also shown are the measurements of Johnson [4]. These were obtained by continuous weighing of the ice slab. The agreement is very good and within the estimated error of the melting rate determinations in this study.

4. CONCLUSIONS

The flow regimes resulting from ice melting in saline water were determined for five ambient water salinity levels, $s_\infty = 35, 30, 22, 17$ and $14‰$. A laminar flow is observed to occur for all levels when the ambient water temperature is low and close to the melting temperature, t_0, at the ambient salinity level. However, two different laminar flow regimes arose. A fully upward laminar flow occurs when $t_\infty < t_m(s_\infty)$, where $t_m(s_\infty)$ is the temperature at which a density extremum occurs at s_∞. These flows are in Region Ia, as shown in

Fig. 1, where both buoyancy effects are acting upwards, and thus the fully laminar upward flow occurs. In Region IIa a laminar bi-directional flow was seen at all of the salinity levels. In this region the thermal buoyancy effect acts downward, in opposition to the saline effect. The outer downflow penetrates deeper into the ambient fluid, and becomes more vigorous as the ambient water temperature is increased. This is seen clearly in Figs. 3(a), 4(a), and 5(a).

At higher ambient temperatures, in Region IIb, the flow regime is dramatically altered. The outer flow splits, remaining downflow on the lower portion of the ice surface, and becoming upflow above. Meanwhile close to the ice surface, is a thin, upward moving layer. This layer becomes turbulent near the top of the surface, before forming an upward rising plume above the surface. The streamwise location at which the outer flow splits is observed to be a function of ambient water temperature at any given salinity level. At lower temperatures the flow splits near the top of the surface, and the splitting point moves downwards as the ambient water temperature increases.

At yet higher ambient temperatures, in Region IIc, the thermal effect dominates the flow over most of the ice surface. The resulting flow is downward and turbulent, and the ice surface melts in an irregular fashion as seen in Figs. 4(d), 5(d) and 7(c).

Ice–liquid interface temperatures were measured using thermocouples embedded in the ice surface. As melting progressed these thermocouples broke out of the surface, at which time the temperature was recorded. These temperatures were then used to infer interface salinities. The interface temperature levels are found to increase monotonically with increasing ambient temperature. On the other hand the interface salinity is found to decrease with increasing t_∞ reflecting a higher melt rate.

Time exposure photographs were also used to determine melt rates and velocity levels for different ambient conditions. The melt rates of $s_\infty = 35‰$ compare well to previously reported measurements at that ambient salinity [4]. The velocity measurements are compared to calculations from [1], and reasonably good agreement is found near the ice surface, where the flow is upward.

Acknowledgements—The authors wish to acknowledge support for this study by the National Science Foundation under grant CME 7721641.

REFERENCES

1. V. P. Carey and B. Gebhart, Transport near a vertical ice surface melting in saline water: some numerical calculations, *J. Fluid Mech.* **107**, 37–55 (1981).
2. B. Gebhart and J. C. Mollendorf, Buoyancy-induced flows in water under conditions in which density extrema may arise, *J. Fluid Mech.* **89**, 673–707 (1978).
3. V. P. Carey, B. Gebhart and J. C. Mollendorf, Buoyancy force reversals in vertical natural convection flows in cold water, *J. Fluid Mech.* **97**, 279–297 (1980).
4. R. S. Johnson, Transport from a melting vertical ice surface in saline water, M.S. thesis, State University of New York at Buffalo (1978).
5. E. G. Josberger and S. Martin, A laboratory and theoretical study of the boundary layer adjacent to a vertical melting ice wall in salt water, *J. Fluid Mech.* **111**, 439–473 (1981).
6. V. P. Carey and B. Gebhart, Transport near a vertical ice surface melting in saline water: experiments at low salinities, *J. Fluid Mech.* **117**, 403–423 (1981).
7. B. Gebhart and T. Audunson, Transport measurements in the arctic ice pack, *Lett. Heat Mass Transfer* **7**, 293–302 (1980).
8. K. Fujino, E. L. Lewis and R. G. Perkin, The freezing point of seawater at pressures up to 100 bars, *J. Geophys. Res.* **79**, 1792 (1974).
9. J. Lyman and R. H. Fleming, Composition of seawater, *J. Marine Res.* **3**, 134 (1940).

TRANSPORT PRES D'UNE SURFACE VERTICALE DE GLACE EN FUSION DANS L'EAU AVEC PLUSIEURS NIVEAUX DE SALINITE

Résumé—On présente des résultats d'une étude expérimentale de l'écoulement naturel adjacent à une surface verticale de glace en fusion dans l'eau saline. Plusieurs salinités ambiantes s_∞ sont étudiées soit 14, 17, 22, 30 et 35‰. Pour chaque salinité, plusieurs températures ambiantes d'eau t_∞ sont considéres, depuis $t_\infty = -1{,}75°C$ quand $s_\infty = 35‰$ jusqu'à $t_\infty = 17°C$ quand $s_\infty = 17‰$.

Des photos du champ d'écoulement montrent différents régimes qui dépendent à la fois de la salinité et de la température ambiante. Pour toutes les salinités considérées ici, l'écoulement est laminaire pour les faibles températures ambiantes. Cet écoulement laminaire est soit ascendant pour les faibles niveaux de salinité, soit bidirectionnel aux plus fortes salinités. Pour des températures ambiantes intermédiaires, l'écoulement est bidirectionnel et laminaire à la partie basse de la surface et ascendant et turbulent à la partie haute. Lorsque la température ambiante est encore augmentée, l'écoulement se sépare avec une couche turbulente se déplaçant vers le bas à la partie basse de la surface, et une autre vers le haut à la partie supérieure. La nature compliquée de cet écoulement est due à l'interaction de deux composantes de forces d'Archimède, celle du gradient de salinité et celle du gradient de température. Ces forces sont de même sens ou opposées selon le niveau de salinités et de températures ambiantes. Chacune de ses forces s'exerce à travers une couche différente de la région totale.

On présente des profils de vitesse mesurés à partir des clichés photographiques et on constate un bon accord avec les résultats analytiques de Carey et Gebhart [1]. Des mesures de températures à l'interface solide–liquide, et les salinités déduites, sont présentées pour différents niveaux de salinités et de températures ambiantes d'eau.

STOFFTRANSPORT AN EINER VERTIKALEN EISFLÄCHE, DIE IN WASSER UNTERSCHIEDLICHEN SALZGEHALTS SCHMILZT

Zusammenfassung—Es werden die Ergebnisse einer experimentellen Untersuchung der auftriebsbedingten Strömung an einer vertikalen Eisfläche, die in Kontakt mit Salzwasser schmilzt, mitgeteilt. Mehrere Salzgehalte, s_∞, des umgebenden Wassers werden untersucht, nämlich 14; 17; 22; 30 und 35‰. Für jeden Salzgehalt werden mehrere Wassertemperaturen t_∞ untersucht, die von $t_\infty = -1{,}75°C$ bei $s_\infty = 35‰$ bis $t_\infty = 17°C$ bei $s_\infty = 17‰$ reichen.

Langzeitaufnahmen des Strömungsfeldes zeigen, daß mehrere völlig unterschiedliche Strömungszustände auftreten, die sowohl vom Salzgehalt des umgebenden Wassers als auch von seiner Temperatur abhängen. Bei allen in der vorliegenden Studie betrachteten Salzgehalten wird bei niedrigen umgebenden Wassertemperaturen laminare Strömung beobachtet. Diese laminare Strömung ist bei niedrigen Salzgehalten aufwärts gerichtet bzw. bei höheren zweifach gerichtet. Bei mittleren Wassertemperaturen ist die Strömung im unteren Bereich der Eisoberfläche laminar und zweifach gerichtet, dagegen turbulent und aufwärtsströmend im oberen Teil der Eisfläche. Bei weiterer Steigerung der Wassertemperatur teilt sich die Strömung in eine turbulente, abwärtsströmende Schicht im unteren Bereich und eine aufwärtsströmende Schicht im oberen Bereich. Der komplizierte Charakter dieser Strömung ist in der Wechselwirkung von zwei Auftriebskomponenten begründet, nämlich den durch Salzgehalt und Temperaturunterschied bedingten. Diese Kräfte sind je nach Salzgehalt und Temperatur gleich- oder entgegengerichtet. Auch wirken beide Kräfte in unterschiedlichen Bereichen der Gesamtgrenzschicht. Geschwindigkeitsprofile, die aus den Langzeitaufnehmen ermittelt wurden, werden angegeben und befinden sich in guter Übereinstimmung mit den analytischen Resultaten von Carey und Gebhart [1]. Gemessene Temperaturen der Phasengrenze und abgeleitete Salzgehalte werden ebenfalls für verschiedene Salzgehalte und Temperaturen des umgebenden Wassers mitgeteilt.

ПЕРЕНОС У ВЕРТИКАЛЬНОЙ ПОВЕРХНОСТИ ЛЬДА В ПРОЦЕССЕ ЕГО ТАЯНИЯ В ОБЪЕМЕ ВОДЫ С РАЗЛИЧНЫМИ СТЕПЕНЯМИ СОЛЕНОСТИ

Аннотация—Представлены результаты экспериментального исследования течения под действием подъемной силы у вертикальной поверхности льда при его таянии в соленой воде. Эксперименты выполнялись с водой различных степеней солености s_∞, а именно: 14, 17, 22, 30 и 35‰. Для каждой степени солености исследования проводились при нескольких значениях температуры воды t_∞: от $t_\infty = -1{,}75°C$ при $s_\infty = 35‰$ до $t_\infty = 17°C$ при $s_\infty = 17‰$.

Покадровая съемка позволяет выявить несколько четко отличающихся режимов течения, зависящих как от степени солености окружающей воды, так и от ее температуры. Показано, что при всех исследуемых степенях солености течение ламинарное при низких температурах воды. При этом оно либо направлено вверх для низких степеней солености, либо происходит в двух направлениях при более высокой солености. Для промежуточных значений температуры воды наблюдаются ламинарное течение в двух направлениях в нижней части поверхности льда и восходящий турбулентный поток в верхней его части. По мере дальнейшего увеличение температуры воды поток разделяется на нисходящий турбулентный в нижней части поверхности льда и восходящий в его верхней части. Сложный характер течения объясняется взаимодействием двух компонентнов подъемной силы, обусловленных градиентами солености и температуры. Они действуют в одном и том же или противоположных направлениях в зависимости от степени солености и температуры воды. Кроме того, их влияние проявляется в пограничных областях различной толщины.

Представлены измеренные по кинокадрам профили скорости и показано, что они хорошо согласуются с аналитическими результатами Кейри и Гебхарта [1]. Приведены также измеренные значения температуры и соответствующие степени солености на границе раздела твердое тело-жидкость для различных степеней солености и температур воды.